



Time-Reversal Based Range Extension Technique for Ultra-wideband (UWB) Sensors and Applications in Tactical Communications and Networking

Technical Report (Quarterly)

to

US Office of Naval Research

875 North Randolph Street

Arlington, VA 22203-1995

for

Grant # N00014-07-1-0529

Prepared by

Robert C. Qiu

(Principal Investigator)

together with

(Contributing Researchers at Wireless Networking Systems Lab)

Nan (Terry) Guo

Yu Song

Peng (Peter) Zhang

Zhen (Edward) Hu

July 16, 2009

Department of Electrical and Computer Engineering

Center for Manufacturing Research

Tennessee Technological University

Cookeville, TN 38505

20091030239

REPORT DOCUMENTATION PAGE

Form Approved
OMB No. 0704-0188

The public reporting burden for this collection of information is estimated to average 1 hour per response, including the time for reviewing instructions, searching existing data sources, gathering and maintaining the data needed, and completing and reviewing the collection of information. Send comments regarding this burden estimate or any other aspect of this collection of information, including suggestions for reducing the burden, to Department of Defense, Washington Headquarters Services, Directorate for Information Operations and Reports (0704-0188), 1215 Jefferson Davis Highway, Suite 1204, Arlington, VA 22202-4302. Respondents should be aware that notwithstanding any other provision of law, no person shall be subject to any penalty for failing to comply with a collection of information if it does not display a currently valid OMB control number.

PLEASE DO NOT RETURN YOUR FORM TO THE ABOVE ADDRESS.

1. REPORT DATE (DD-MM-YYYY) 16-04-2009			2. REPORT TYPE Technical Report (Quarterly)		3. DATES COVERED (From - To) April 16, 2009---July 16, 2009	
4. TITLE AND SUBTITLE Time-Reversal Based Range Extension Technique for Ultra-wideband (UWB) Sensors and Applications in Tactical Communications and Networking					5a. CONTRACT NUMBER	
					5b. GRANT NUMBER N00014-07-1-0529	
					5c. PROGRAM ELEMENT NUMBER	
6. AUTHOR(S) Qiu, Robert C.; Guo, Nan; Song, Yu; Zhang, Peng; Hu, Zhen					5d. PROJECT NUMBER	
					5e. TASK NUMBER	
					5f. WORK UNIT NUMBER	
7. PERFORMING ORGANIZATION NAME(S) AND ADDRESS(ES) Tennessee Technological University 115 W. 10th Street Cookeville, TN 38501					8. PERFORMING ORGANIZATION REPORT NUMBER	
9. SPONSORING/MONITORING AGENCY NAME(S) AND ADDRESS(ES) US Office of Naval Research 875 North Randolph Street Arlington, VA 22203-1995					10. SPONSOR/MONITOR'S ACRONYM(S) ONR	
					11. SPONSOR/MONITOR'S REPORT NUMBER(S) 07PR05074-00	
12. DISTRIBUTION/AVAILABILITY STATEMENT release for public distribution.						
13. SUPPLEMENTARY NOTES						
14. ABSTRACT This report summarizes our recent UWB testbed development work with specific progresses in measurement of current system, 2 by 1 MISO system implementation and waveform optimization. The radio testbed is in evolution toward a wideband MIMO system. MISO time reversal concept has been successfully demonstrated based on an energy detector receiver. The receiver is being modified to become the coherent type. Then multiple receiver chains will be considered.						
15. SUBJECT TERMS UWB, testbed, time reversal, range extension, sensors, multi-GHz wideband, cognitive radio						
16. SECURITY CLASSIFICATION OF:			17. LIMITATION OF ABSTRACT UU	18. NUMBER OF PAGES 24	19a. NAME OF RESPONSIBLE PERSON Francis Otuonye	
a. REPORT U	b. ABSTRACT U	c. THIS PAGE U			19b. TELEPHONE NUMBER (Include area code) 931-372-3374	

REPORT OF INVENTIONS AND SUBCONTRACTS

(Pursuant to "Patent Rights" Contract Clause) (See Instructions on back)

*Form Approved
OMB No. 9000-0095
Expires Jan 31, 2008*

The public reporting burden for this collection of information is estimated to average 1 hour per response, including the time for reviewing instructions, searching existing data sources, gathering and maintaining the data needed, and completing and reviewing the collection of information. Send comments regarding this burden estimate or any other aspect of this collection of information, including suggestions for reducing the burden, to the Department of Defense, Executive Services Directorate (9000-0095). Respondents should be aware that notwithstanding any other provision of law, no person shall be subject to any penalty for failing to comply with a collection of information if it does not display a currently valid OMB control number.

PLEASE DO NOT RETURN YOUR COMPLETED FORM TO THE ABOVE ORGANIZATION. RETURN COMPLETED FORM TO THE CONTRACTING OFFICER.

1. a. NAME OF CONTRACTOR/SUBCONTRACTOR Tennessee Technological University		c. CONTRACT NUMBER N00014-07-1-0529		3. TYPE OF REPORT (X one) <input checked="" type="checkbox"/> a. INTERIM <input type="checkbox"/> b. FINAL	
b. ADDRESS (Include ZIP Code) 115 W. 10th Street Cookeville, TN 38501		2. a. NAME OF GOVERNMENT PRIME CONTRACTOR US Office of Naval Research		4. REPORTING PERIOD (YYYYMMDD) a. FROM 20090416 b. TO 20090716	
d. AWARD DATE (YYYYMMDD) 20070116		d. AWARD OATE (YYYYMMDD) 20070416			

SECTION I - SUBJECT INVENTIONS

5. "SUBJECT INVENTIONS" REQUIRED TO BE REPORTED BY CONTRACTOR/SUBCONTRACTOR (If "None," so state)		DISCLOSURE NUMBER, PATENT APPLICATION SERIAL NUMBER OR PATENT NUMBER c.	ELECTION TO FILE PATENT APPLICATIONS (X)		CONFIRMATORY INSTRUMENT OR ASSIGNMENT FORWARDED TO CONTRACTING OFFICER (X) e.
NAME(S) OF INVENTOR(S) (Last, First, Middle Initial)	TITLE OF INVENTION(S) b.		(1) UNITED STATES (a) YES (b) NO	(2) FOREIGN (a) YES (b) NO	
None					
f. EMPLOYER OF INVENTOR(S) NOT EMPLOYED BY CONTRACTOR/SUBCONTRACTOR	g. ELECTED FOREIGN COUNTRIES IN WHICH A PATENT APPLICATION WILL BE FILED				
(1) (a) NAME OF INVENTOR (Last, First, Middle Initial)	(2) (a) NAME OF INVENTOR (Last, First, Middle Initial)	(1) TITLE OF INVENTION		(2) FOREIGN COUNTRIES OF PATENT APPLICATION	
(b) NAME OF EMPLOYER					
(c) ADDRESS OF EMPLOYER (Include ZIP Code)	(c) ADDRESS OF EMPLOYER (Include ZIP Code)				

SECTION II - SUBCONTRACTS (Containing a "Patent Rights" clause)

6. SUBCONTRACTS AWARDED BY CONTRACTOR/SUBCONTRACTOR (If "None," so state)					
NAME OF SUBCONTRACTOR(S) a.	ADDRESS (Include ZIP Code) b.	SUBCONTRACT NUMBER(S) c.	FAR "PATENT RIGHTS" d.		SUBCONTRACT DATES (YYYYMMDD) f.
			(1) CLAUSE NUMBER	(2) DATE (YYYYMM)	
None					
			DESCRIPTION OF WORK TO BE PERFORMED UNDER SUBCONTRACT(S) a.		(1) AWARD (2) ESTIMATED COMPLETION

SECTION III - CERTIFICATION

7. CERTIFICATION OF REPORT BY CONTRACTOR/SUBCONTRACTOR (Not required if: (X as appropriate))		<input type="checkbox"/> SMALL BUSINESS or	<input type="checkbox"/> NONPROFIT ORGANIZATION
I certify that the reporting party has procedures for prompt identification and timely disclosure of "Subject Inventions," that such procedures have been followed and that all "Subject Inventions" have been reported.			
a. NAME OF AUTHORIZED CONTRACTOR/SUBCONTRACTOR OFFICIAL (Last, First, Middle Initial) Otuonye, Francis	b. TITLE Associate Vice President	c. SIGNATURE N/A	d. DATE SIGNED

DD FORM 882, JUL 2005

PREVIOUS EDITION IS OBSOLETE.

Acknowledgment

This work has been improved by discussions with S. K. Das (ONR), B. M. Sadler (ARL), R. Ulman (ARO), and L. Lunardi (formerly with NSF). K. Currie (CMR, TTU) has provided a lot of support for this project. S. Parke (ECE, TTU) has supported our research in different ways. We also want to thank P. K. Rajan for helpful discussions.

Executive Summary

This report summarizes our recent UWB testbed development work with specific progresses in measurement of current system, 2 by 1 MISO system implementation and waveform optimization. The radio testbed is in evolution toward a wideband MIMO system. MISO time reversal concept has been successfully demonstrated based on an energy detector receiver. The receiver is being modified to become the coherent type. Then multiple receiver chains will be considered.

Contents

I	System Development	1
1	Introduction	3
2	Measurement of Channel and System Performance (BER)	5
2.1	Compressed Sensing Based Impulse Response Measurement	5
2.2	Error Rate Measurement	7
3	2 by 1 MISO System Development	9
3.1	Transmitter Implementation	9
3.1.1	Transmitter Architecture and Components	9
3.1.2	SMA Cable Parameters	10
3.2	Wideband Receiver	16
3.2.1	Receiver Architecture and Components	16
3.2.2	Products Selection	17
3.2.3	Quadrature Demodulator ADL5380 Test	21
II	Theoretical Work	29
4	Wideband Waveform Optimization for Multiple Input Single Output (MISO) Cognitive Radio Using Time Reversal	31
4.1	Wideband Waveform Optimization	31

4.2	Numerical Results	36
4.3	Discussion	37

Part I

System Development

Chapter 1

Introduction

After two years of testbed development we have reached a primary goal. This goal is demonstrating how UWB waveform level precoding affects performance. However, there are still many work items left in the waveform precoding framework. Our recent development work has been focused on hardware improvement, adding new features and system measurement. Work reported in Part I reflects our effort toward a wideband MIMO system. Receiver change from current noncoherent type to coherent type is a great deal, and the work has been started.

Meanwhile, we have continued in forward looking and attempting to apply the latest theoretical results to the testbed. For example, compressed sensing, a new concept of signal sampling, has been considered in channel measurement to improve accuracy at lower sampling rate. In addition, our arbitrary waveform generator implementation is also directed by our ongoing waveform optimization work.

Chapter 2

Measurement of Channel and System Performance (BER)

2.1 Compressed Sensing Based Impulse Response Measurement

In this experiment, we are going to measure the impulse response of a differentiator using the compressed sensing based method proposed in paper [1]. Thanks to arbitrary waveform generator (AWG) and digital phosphor oscilloscope (DPO), we are able to perform a real-world experiment without too much concern on setting up the hardware. The experiment set-up is illustrated in Fig. 2.1. AWG generates a probing pulse as input to the device whose output is captured by DPO using only 10% of Nyquist rate. As mentioned before, PN sequence at Nyquist rate is a good source of probing pulse. The captured data is then processed by basis pursuit (BP) algorithm [2] in Matlab to reconstruct the impulse response of the device which is represented in Nyquist rate. The Nyquist rate waveform and BP reconstructed waveform will be compared in both time domain and frequency domain to show the accuracy of the proposed measurement approach.

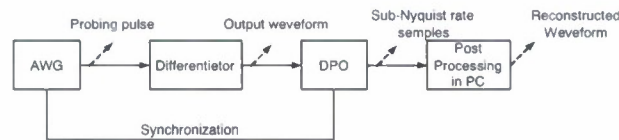


Figure 2.1: Experiment setup using AWG and DPO.

Our interested frequency band of the differentiator is below 3.125 GHz and the Nyquist rate is set to 6.25 Gsps. Average is applied in DPO to eliminate the Gaussian noise. We will first get a 6.25 Gsps waveform at DPO by sending a 6.25 Gsps mono-eye pulse from AWG. This output will be considered as the Nyquist rate waveform samples. Then, we will send a 800 ns long PN sequence at 6.25 Gsps and get 625 Msps waveform samples at DPO (Fig. 2.2). These waveform samples will then be processed by BP in Matlab to get a reconstructed waveform at 6.25 Gsps. Fig. 2.3 and Fig. 2.4 show the results of the reconstructed waveform and Nyquist rate waveform in time domain and frequency domain, respectively. It can be seen that both results coincide with each other with high accuracy. The mean square error (MSE) of reconstructed waveform is 2.08%. Some errors exist because of DPO's internal interference.

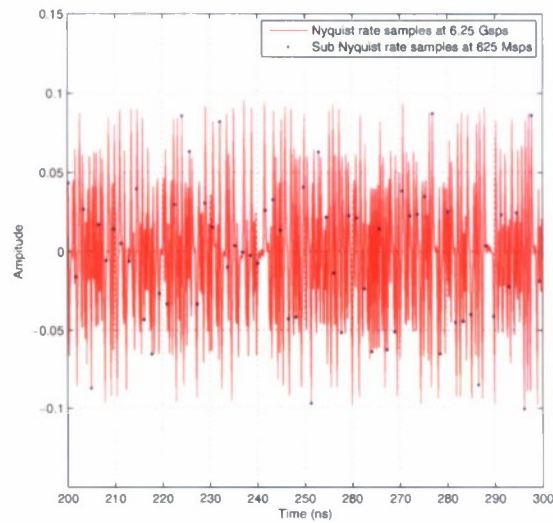


Figure 2.2: Illustration of Nyquist rate waveform samples and sub Nyquist rate waveform samples. Nyquist rate waveform is used for illustration. Only Sub Nyquist rate samples is used for reconstruction.

Figure 2.3: Time domain comparison of reconstructed waveform and Nyquist rate waveform.

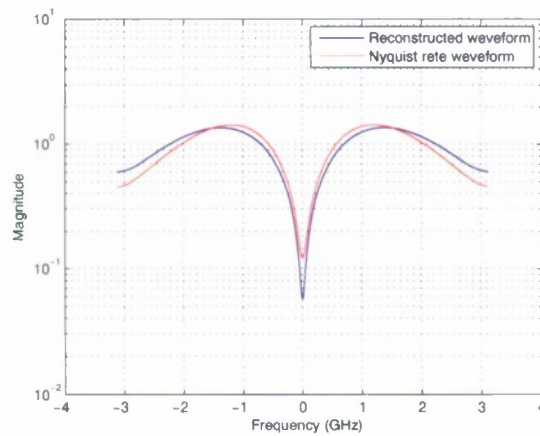


Figure 2.4: Frequency domain comparison of reconstructed waveform and Nyquist rate waveform.

2.2 Error Rate Measurement

The BER measurement is done in an off-line manner in Matlab. The demodulated digital data is acquired by Agilent 16803 Logic Analyzer (LA) at FPGA data pins directly. Then, the data is loaded in Matlab and processed to get the BER. The data rate is 6.25 Mb/s for the communication system and the sampling clock of the LA is 12.5 MHz, with an over sampling factor of two. This clock is connected to Pod A1 of LA. Fig. 2.6 shows the bus/signals we want to acquire. There are 2 signals in the picture, the "clk" is a 6.25 MHz clock corresponding the data rate, while the "sync1" is the synchronization indicator meaning the start of data output. "data" is the output source signal. Another important setup is the trigger setup. We set the trigger as the start of the frame, which means that when the output data comes with 20 '0's following a '1', the system starts to sample.

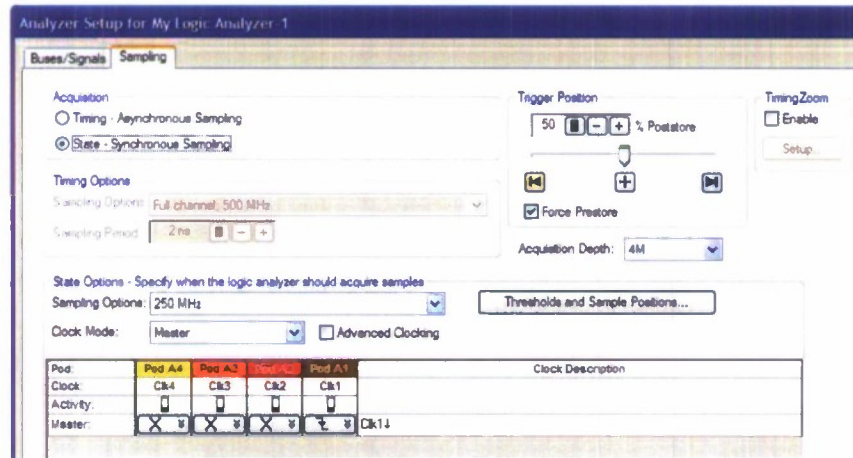


Figure 2.5: Logic analyzer sampling clock setup.

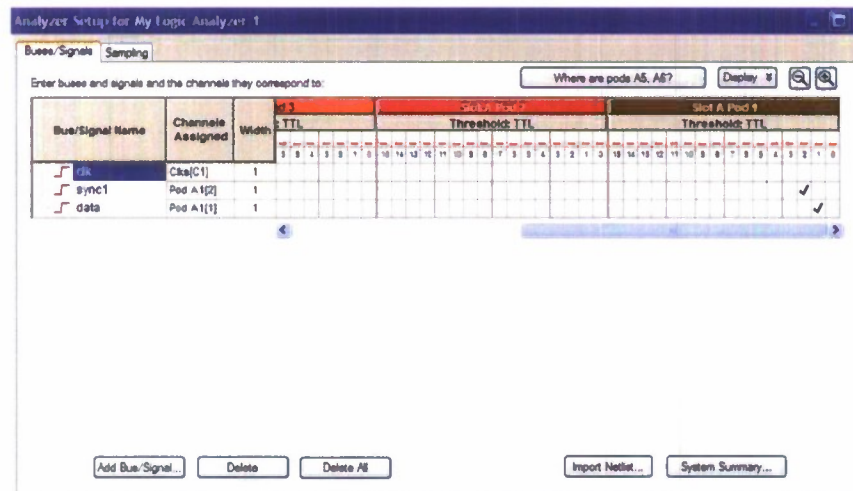


Figure 2.6: Logic analyzer bus/signal setup..

In order to ease the work in Matlab, we define the frame structure as illustrated in Fig. 2.7. The data acquisition consists of two steps: frame head acquisition and data pattern acquisition. Since data is generated by repeating

Table 2.1: Comparison in frame loss rate

Time Reversal Power (dBm)	-3.8	-0.8	2.2
Frame Loss Rate	83%	22%	12%
Pulse Power (dBm)	-3.2	-0.2	2.8
Frame Loss Rate	99%	95%	81%

the feature pattern '1010110011110000' 960 times after all '0's idle sequence, the idle sequence together with one feature pattern can be used to detect the frame head.

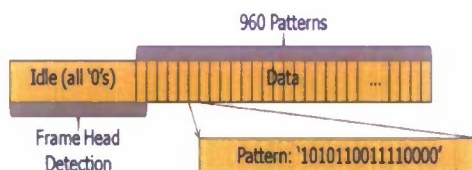


Figure 2.7: Frame Structure

After recognizing the data pattern, we can start the BER measurement. Due to the equipment limitation, we cannot measure SNR at the receiver. Alternatively, we use the received power as a metric for BER performance. Note, since the ADC has clipping effect, the received amplitude should be lower than the range of ADC, so that the clipping will not affect the signal's power.

The received data is compared with sent data to get BER. '000000000000001010110011110000' is used for frame head detection. 3 bits of errors can be tolerated. A frame head detection failure might be caused by synchronization problem. After that, the data part is compared with local data and get the BER. We are interested in 2 statistics, frame loss rate and conditional BER.

Since we know the number of the total frames that were sent, we only need to know the total number of frames that were received to get the frame loss rate. This helps us to analysis the performance of receiver's synchronization.

The conditional BER is the BER under the condition that the frame head is successfully detected. If the frame head is not detected, the data in the frame cannot be achieved to compare with the local data. So the BER we get is the BER under the synchronized condition.

We compare the results with and Time Reversal system and pulse system. Table 2.1 shows the comparison in frame loss rate.

It is obvious that Time Reversal system out performs pulse system. However, the pulse system shows some problems. Since the frame loss rate is still very high when pulse power is high. This might be caused by synchronization, which is going to be figured out.

Chapter 3

2 by 1 MISO System Development

3.1 Transmitter Implementation

3.1.1 Transmitter Architecture and Components

For this quarter, A 2 by 1 MISO system was being designed and implemented, Figure 3.1 shows the diagram of the transmitter. The main components include the following: (1) One FPGA as the main digital part. (2) One DAC board capable of generating two output waveforms. (3) Two identical modulators working from 400 MHz to 6 GHz. (4) Two identical power amplifiers. (5) A local oscillator. (6) A power splitter to convert LO signal to two identical signals for the two modulators. (7) Two identical wideband antennas (8) A bunch of SMA cables with reasonable length and characteristics.

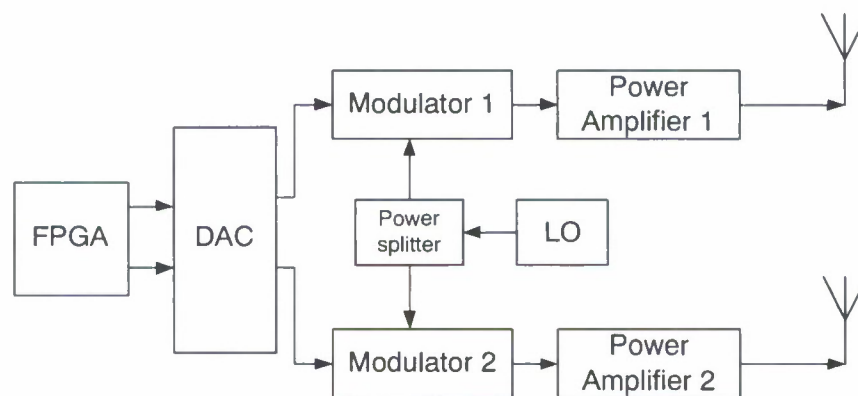


Figure 3.1: Diagram of the transmitter for a 2 by 1 MISO system.

The receiver currently being used is energy detection based, and only with one receive antennas. But the MISO system is designed to explore the benefit of multi-antennas in real life, If there is a gain for 2 antennas at the transmitter side, then it will be OK.

3.1.2 SMA Cable Parameters

All modules are connected by SMA cables in the off-the-shelf components based testbed. Since cables always have certain reflections and attenuations, the signal quality will be affected in certain level. In order to ensure the signal quality, SMA cable parameters such as S11 and S21 are measured.

Most coaxial cables have a characteristic impedance of either 50, 52, 75, or 93-ohm. The RF industry uses standard type-names for coaxial cables, a series of standard types of coaxial cable were specified for military uses, in the form "RG-#" or "RG-#/U". Figure 3.2 shows the table of RG standards type.

type	approx. impedance [ohms]	core	dielectric			overall diameter		braid	velocity factor	comments
			type	[in]	[mm]	in	mm			
RG-8U	75	1.0 mm	Solid PE	0.185	4.7	0.270	8.4	double	0.75	Low loss at high frequency for cable television, satellite television and cable modems
RG-6/UQ	75		Solid PE			0.298	7.62	quad		This is "quad shield RG-6". It has four layers of shielding, regular RG-6 only has one or two
RG-8U	50	2.17 mm	Solid PE	0.285	7.2	0.405	10.3			Amateur radio. Thicknet (10BASE5) is similar
RG-9U	51		Solid PE			0.420	10.7			
RG-11/U	75	1.63 mm	Solid PE	0.285	7.2	0.412	10.5		0.66	Used for long drops and underground conduit
RG-58/U	50	0.9 mm	Solid PE	0.116	2.9	0.195	5.0	single	0.66/0.78	Used for radiocommunication and amateur radio, thin Ethernet (10BASE2) and NIM electronics. Common.
RG-59/U	75	0.81 mm	Solid PE	0.146	3.7	0.242	6.1	single	0.66	Used to carry baseband video in closed-circuit television, previously used for cable television. Generally it has poor shielding but will carry an HQ HD signal or video over short distances.
RG-60/U	50	1.024 mm	Solid PE			0.425	10.8	single		Used for high-definition cable TV and high-speed cable internet
RG-62/U	92		Solid PE			0.242	6.1	single	0.84	Used for ARCNET and automotive radio antennas.
RG-62A	93		ASP			0.242	6.1	single		Used for NIM electronics
RG-174/U	50	0.48 mm	Solid PE	0.100	2.5	0.100	2.55	single	0.66	Common for wifi pigtails: more flexible but higher loss than RG58; used with LEMO 00 connectors in NIM electronics.
RG-178/U	50	7*0.1 mm (Ag plated Cu clad Steel)	PTFE	0.033	0.84	0.071	1.8	single	0.69	
RG-179/U	75	7*0.1 mm (Ag plated Cu)	PTFE	0.063	1.6	0.068	2.5	single	0.67	VGA RGBHV
RG-213/U	50	7*0.0296 in Cu	Solid PE	0.285	7.2	0.405	10.3	single	0.66	For radiocommunication and amateur radio, EMC test antenna cables. Typically lower loss than RG58. Common.
RG-214/U	50	7*0.0296 in	PTFE	0.285	7.2	0.425	10.8	double	0.66	

Figure 3.2: Tabel of RG standards.

- CABLE SMA/SMA 6" RG-316DS

Manufacturer: Emerson Network Power Connectivity Solutions
 Length: 6.0"
 Color: White
 RG Type: RG-316 DS
 Connector Type: SMA Male to SMA Male
 Features: Shielded

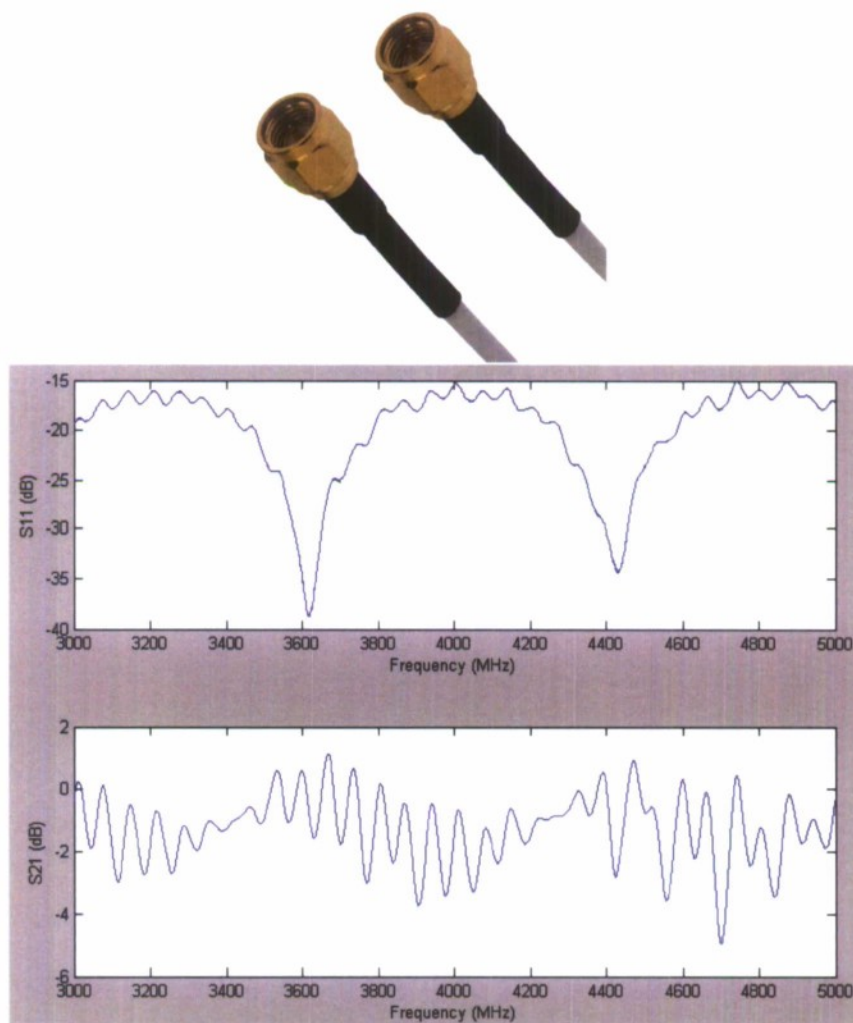


Figure 3.3: CABLE SMA/SMA 6" RG-316DS.

- CABLE SMA/SMA 24" RG-316DS

Manufacturer: Emerson Network Power Connectivity Solutions

Length: 24.0" (609.6mm)

Color: White

RG Type: RG-316 DS

Connector Type: SMA Male to SMA Male

Features: Shielded

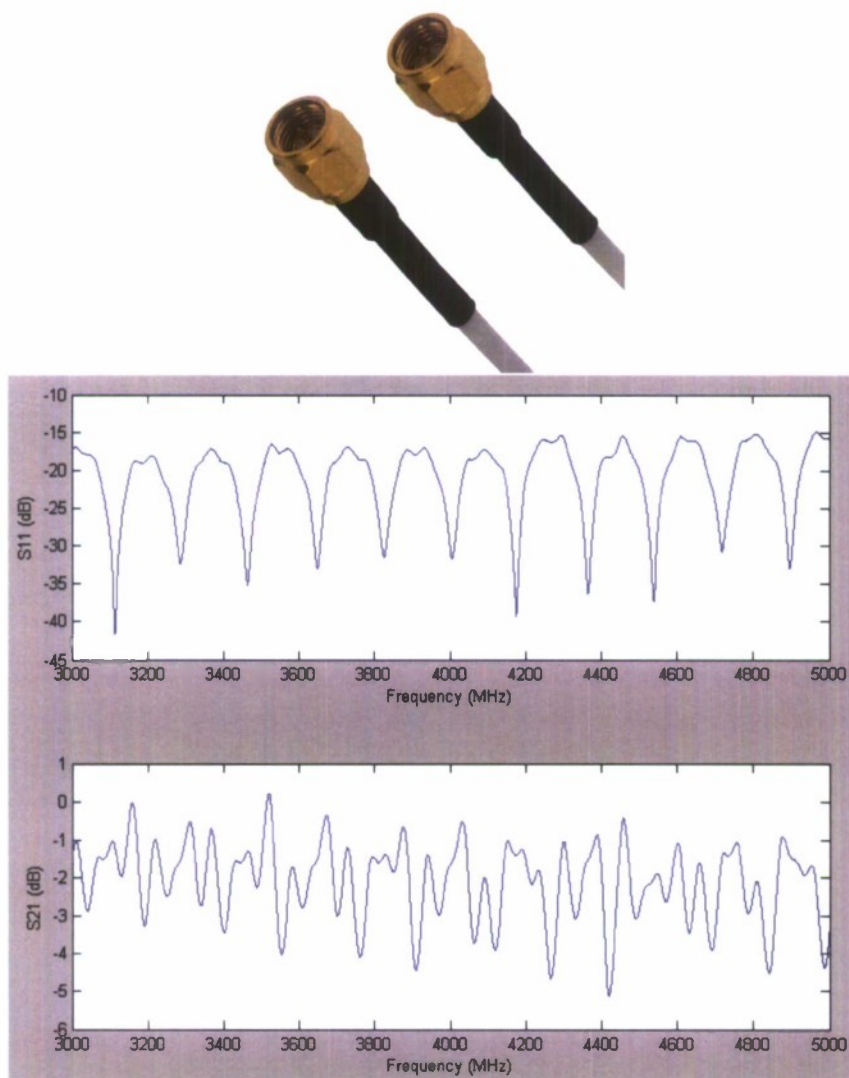


Figure 3.4: CABLE SMA/SMA 24" RG-316DS.

- CABLE SMA PLUG-PLUG HF-.086 8"

Length: 8.0" (203.2mm)
Color: Gray
RG Type: Hand Formable .086
Connector: Type SMA Male to SMA Male
Features: Shielded

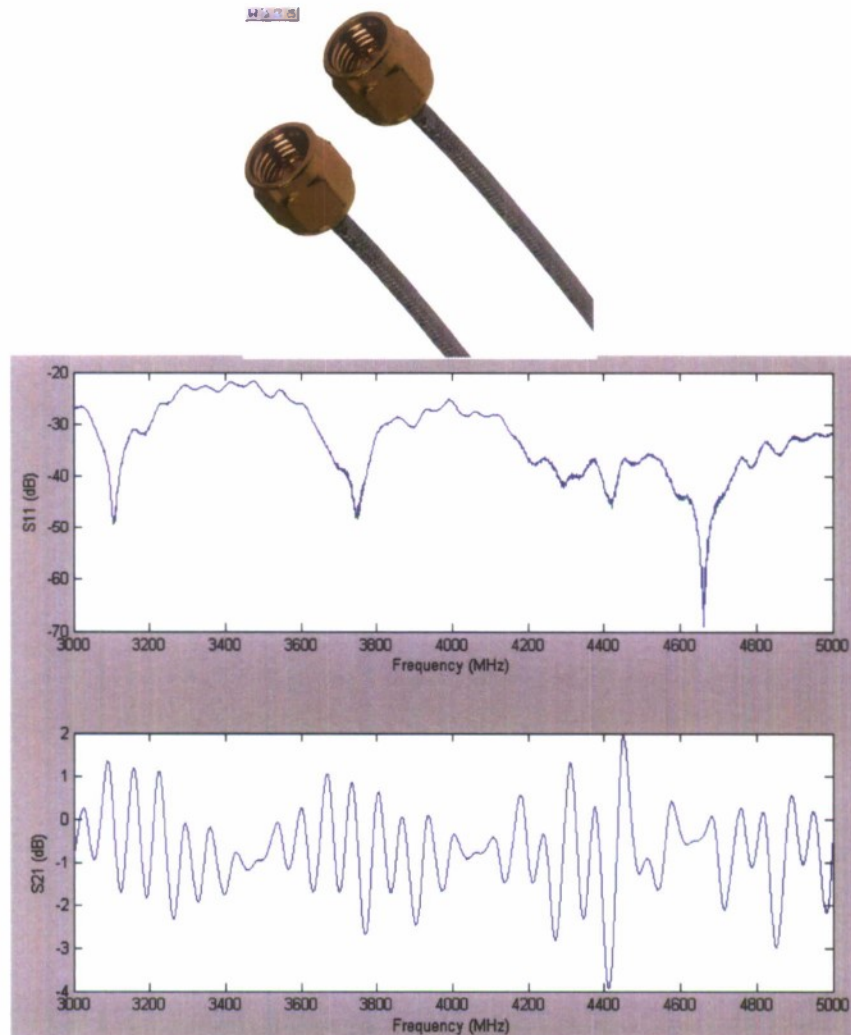


Figure 3.5: CABLE SMA PLUG-PLUG HF-.086 8" .

- CABLE SMA PLUG-PLUG HF-.141 8"

Length: 8.0" (203.2mm)
Color: Gray
RG Type: Hand Formable .141

Connector: Type SMA Male to SMA Male
Features: Shielded

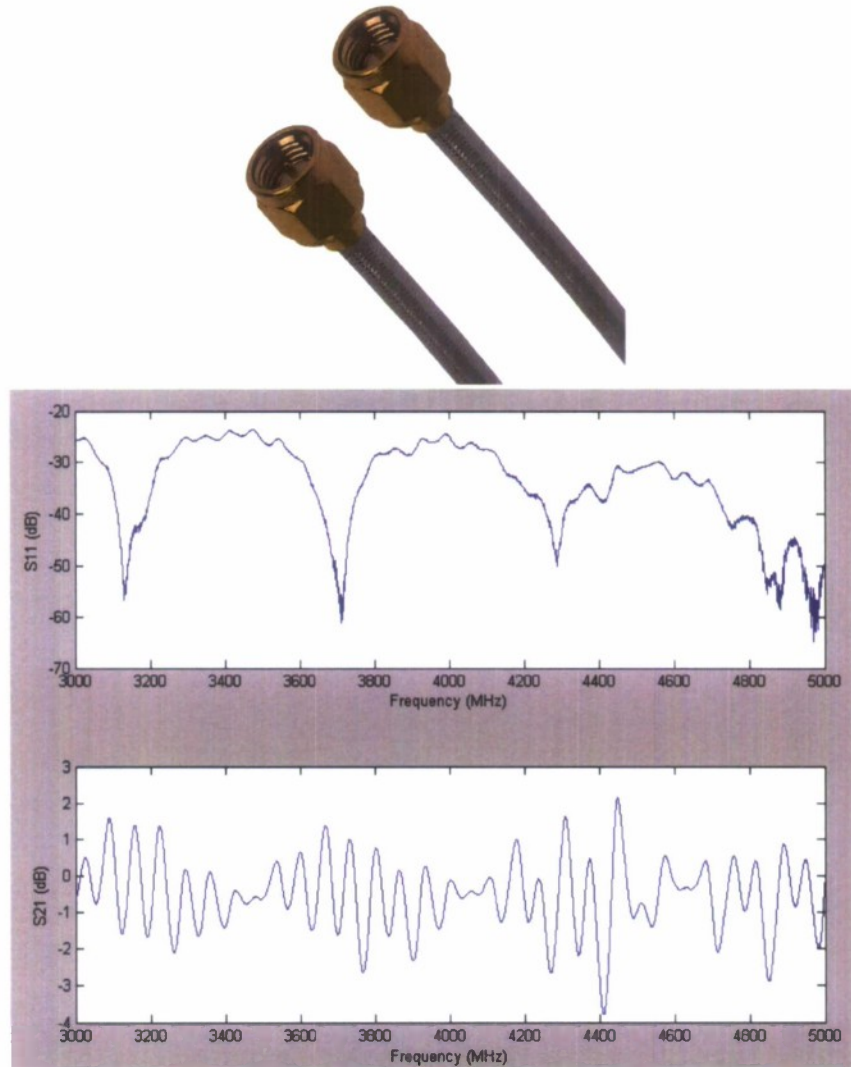


Figure 3.6: CABLE SMA PLUG-PLUG HF-.141 8"

- CABLE SMA PLUG-PLUG HF-.141 12"

Length: 12.0" (304.8mm)
Color: Gray
RG Type: Hand Formable .141
Connector: Type SMA Male to SMA Male
Features: Shielded

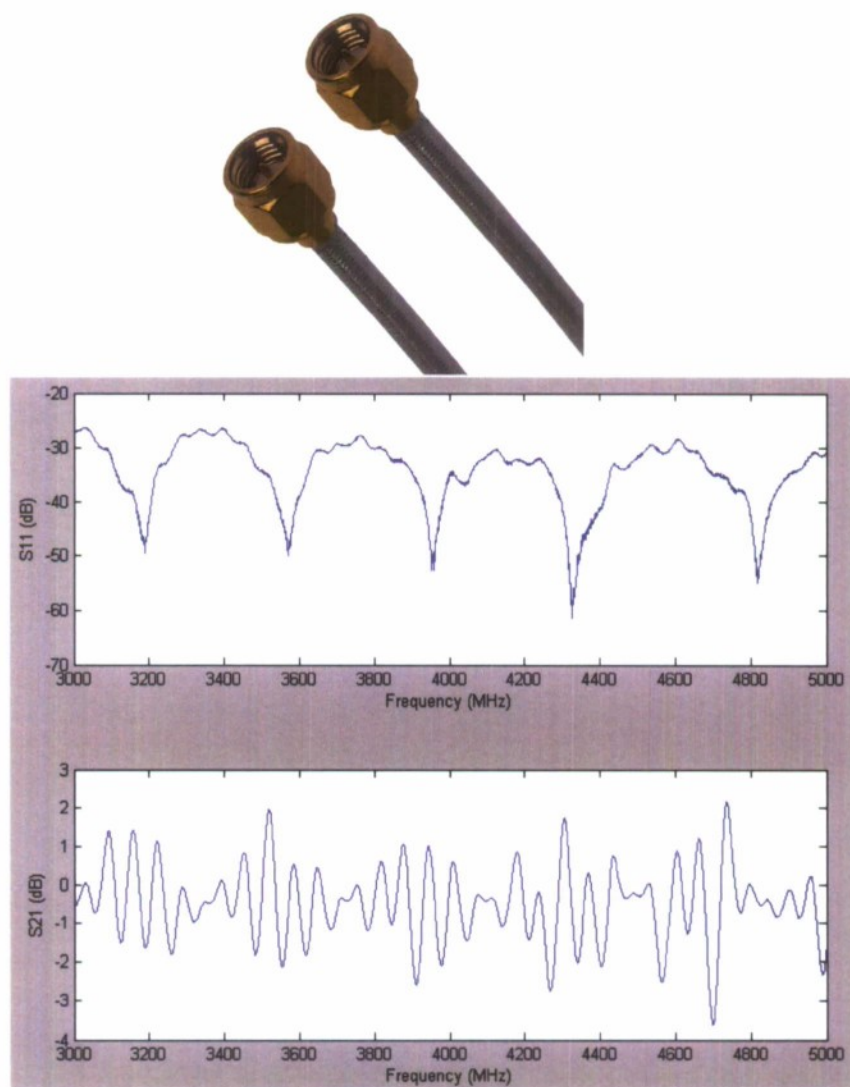


Figure 3.7: CABLE SMA PLUG-PLUG HF-.141 12” .

- SMA MALE TO SMA MALE- 18GHz PRECISION TEST CABLE ASSEMBLY- 120 INCHES

Manufacturer: Pasternack Enterprises
Length: 120.0" (3048mm)
Color: Blue
RG Type: Pasternack Precision
Connector Type: SMA Male to SMA Male
Features: Shielded



PE300 - SMA Male to SMA Male

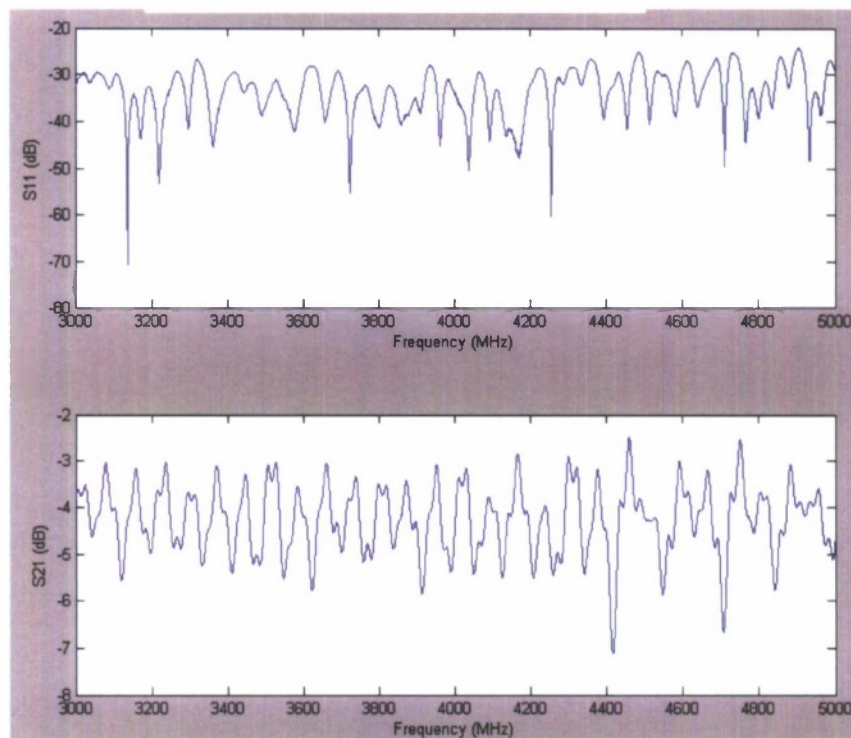


Figure 3.8: Pasternack 18GHz PRECISION TEST CABLE ASSEMBLY- 120 INCHES .

3.2 Wideband Receiver

3.2.1 Receiver Architecture and Components

A wideband coherent receiver is under consideration, it mainly includes three parts, the RF section, mixed signal and digital processing unit.

(1) The RF can be built with off-the-shelf components, which include a bandpass filter, low noise amplifier (LNA), a wideband quadrature demodulator, two low pass filters and certain AGC components.

(2) The mixed signal part is mainly the high speed AD converter, for a wideband signal such as 1 GHz, the AD sampling rate should be at least 3 Gsps, and there should be two of them for both in-phase signal and quadrature-phase signal.

(3) The digital part should be capable of receive the high speed digital signals from ADC and do processing at a high speed. thus the connection between the two parts will be a problem, and the processing capability will be another issue that may need careful consideration.

For the RF part, there are enough components we can choose from. the hard part is the high speed ADCs and high performance digital processing part as well as the high speed connection between them.

3.2.2 Products Selection

Currently, there are the following 5 options for high speed ADC board and FPGAs integration solution.

Option 1: - ADC512 along with a PCI carrier board FPE650 [3].

This product is from Curtiss-Wright Controls Embedded Computing /cwccmbedded.

As Figure 3.9 shows, the ADC512 is a dual channel 3 GSPS analog input FPGA Mezzanine Card (FMC) based on the VITA 57 specification. This specification allows I/O devices to be directly coupled to a host FPGA. On the ADC512, the two ADC devices connect through the high bandwidth FMC connector to an FPGA-based host board.

The ADC512 can be fitted to FMC hosts like Curtiss-Wrights FPE650, shown as Figure 3.10. The FPE650 is a quad FPGA processor card which combines high-performance and high-bandwidth I/O in a flexible format. It includes four fully user programmable FPGA nodes and are arranged in two FPGA node pairs; two are associated with front panel mezzanine sites. Apart from connectivity, the main difference between the FPGA node pairs is the memory architecture. The FPGA nodes are built with 4 Xilinx SX95T platforms.

Option 2: - SMT702 Dual 3GSPS, 8-bit ADC PXI Express Board [4].

This product is from Sundance, Inc.

The SMT702 is a PXI Express Peripheral Module (3U), which integrates two 3 Gsps 8-bit ADCs, a clock circuitry, 2 banks of 1GByte DDR2 Memory each and a Xilinx Virtex5 LX110T-3 FPGA, under the 3U format. The good news for this product is it can be standalone and with a number of general I/Os. Figure 3.11 shows the picture and diagram of SMT702.

For interconnections with other digital processing modules, there are SHB connector and RSL (Rocket I/O serial link) connector, both are come from Samtec, Inc. so we may connect it with others high performance computing system.

Option 3: - BenADC-3G along with PBenONE-PCIe carrier board [5].

This product is from nallatech.

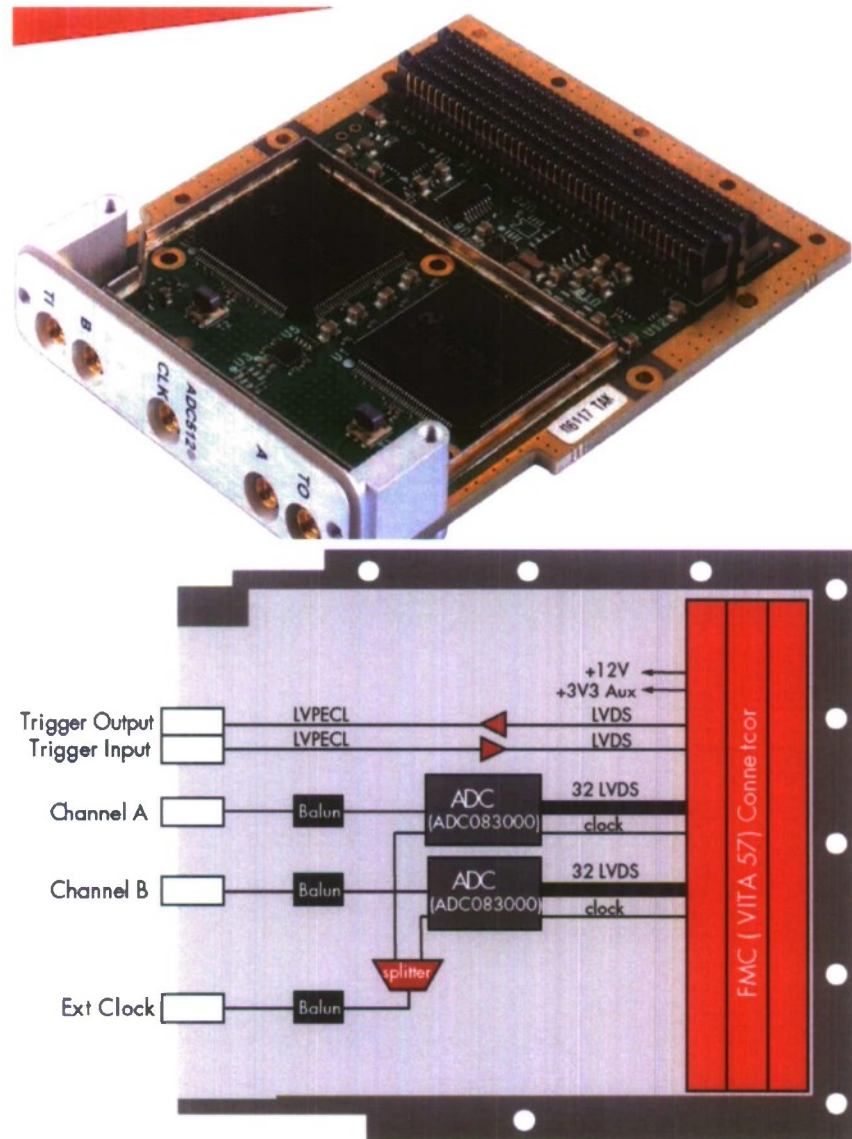


Figure 3.9: ADC512 board picture and functional diagram.

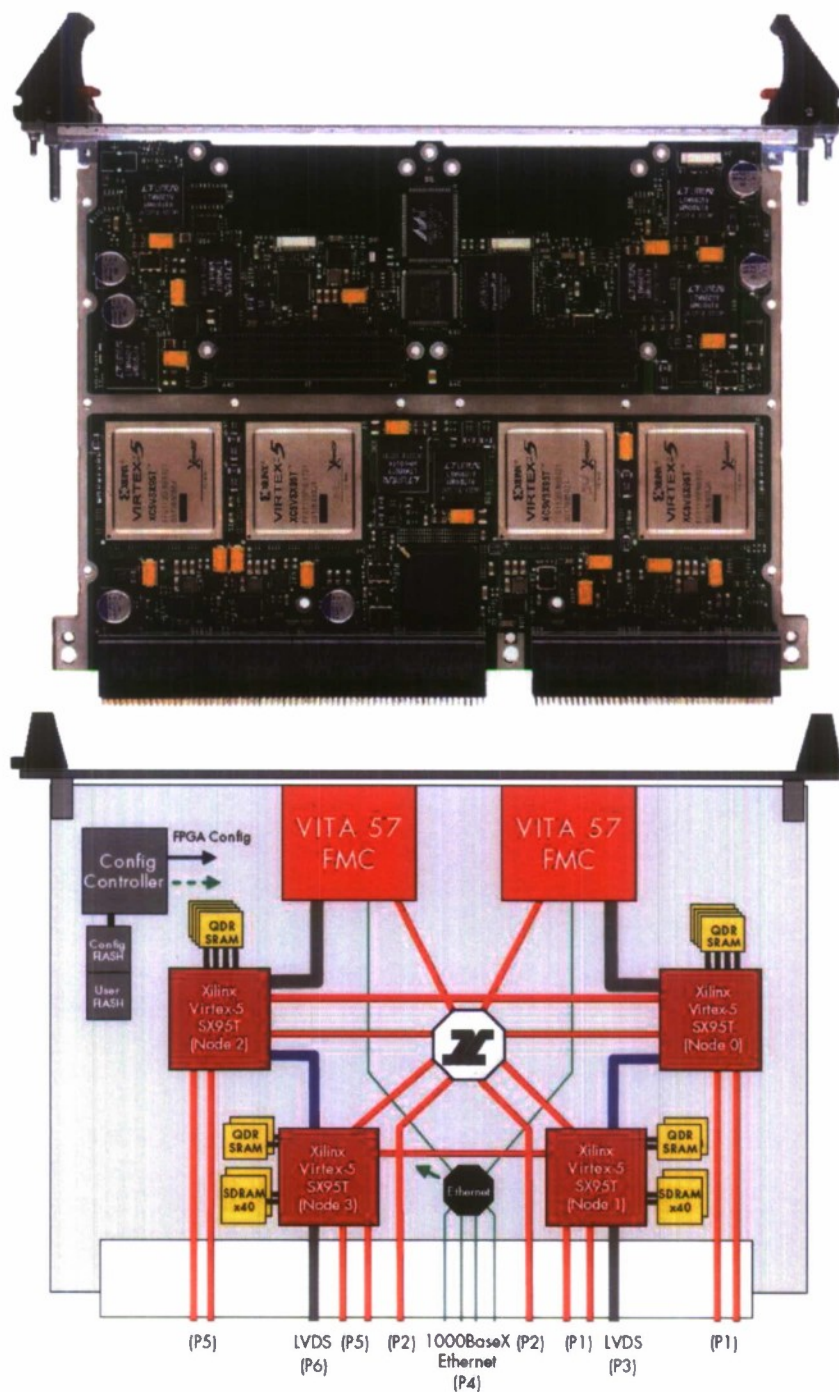


Figure 3.10: FPE650 board picture and functional diagram.

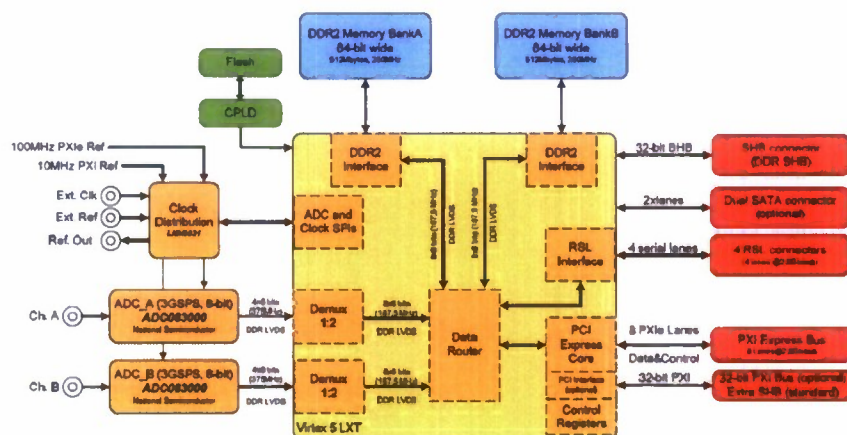
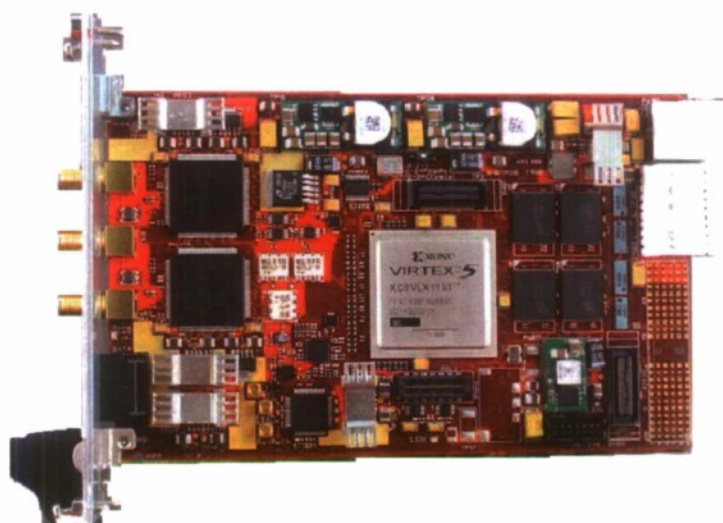


Figure 3.11: SMT702 board picture and functional diagram.

The BenADC-3G module combines a Xilinx Virtex-4 FPGA with two National Semiconductor 8-bit 3 GSPS ADCs providing users with a powerful data acquisition and processing platform. Each ADC083000 can achieve up to 7.2 effective number of bits (ENOB), 45 dB signal-to-noise ratio (SNR) and 58 dB spurious free dynamic range (SFDR) when sampling a 748 MHz input signal at 3 GSPS. Trigger and clock signal inputs allow simultaneous sampling of both channels. Figure 3.12 shows the picture of BenADC-3G.

But a carrier card such as our BenONE-PCIe board is required to host the 3G module, the BenONE-PCIe provides a powerful PCI Express computing platform for high performance FPGA development. Featuring a DIME-II expansion slot, the BenONE-PCIe motherboard supports multiple analog and digital I/O interfaces, memory types, and Xilinx user FPGAs on a single 8-lane PCI Express card. Figure 3.13 shows the picture of BenONE-PCIe.

Option 4: - Neptune-V5 VXS Dual Channel 2 Gsps ADC Digitizer [6].

This product is from TEK Microsystems Inc.

The Neptune-V5 VXS is an ANSI VITA 41-compliant dual channel high speed digitizer board based on the QuiXilica V5 architecture from TEK Microsystems. It embeds 2 channels 10 bit 2.2 Gsps ADC, 3 Xilinx Virtex-5 SXT, LXT or FXT FPGAs, with 1 GB DDR3 Memory per FPGA. For the connection, it has dual 4x Full Duplex VXS Links, 2x Full Duplex VITA 41.6 Ethernet Links and QuiXstart FPGA Configuration System. Figure 3.14 shows its picture and architecture.

The Neptune-V5 VXS is not supposed to be used as standalone, usually it fits to a carrier card.

Looks like Figure 3.15 shows, VXS is also known as VITA 41((VME International Trade Association)), is a computing standard that introduces serial switch fabric technology into the VME64(VMEbus is a computer bus standard) architecture, VXS enabled systems to deliver bandwidths of 2.5 GBps per slot. The VXS base specification describes two types of cards payload and switch and a corresponding backplane slot for each. The connector's current capacity is about 1A per pin and offered a power intake to a slot of 35W from the primary +5V supply.

Option 5: - X5-GSPS PCI Express XMC Module with Dual channel 1.5 GSPS, 8-bit Digitizer [7].

This product is from Innovative Integration.

The X5-GSPS is an XMC I/O module featuring dual channels of 1.5 GSPS 8-bit digitizing with a Virtex5 FPGA computing core, DRAM and SRAM memory, and eight lane PCI Express host interface. A Xilinx Virtex5 SX95T or LX155T with 512 MB DDR2 DRAM and 4MB QDR-II memory provides a very high performance DSP core for demanding applications. and Figure 3.16 shows its picture and its architecture.

The connection type of this product is XMC PCI express, and there is a 16 bits digital I/Os used as Rocket I/Os with a speed up to 2.5 Gbps.

3.2.3 Quadrature Demodulator ADL5380 Test

For the front-end of a coherent receiver, a wideband quadrature demodulator ADL5380 from Analog Device has been chosen and the evaluation board ADL5380-29A-EVALZ for operation from 3GHz to 4GHz has been tested.

The ADL5380 is a high performance quadrature I-Q demodulator that covers an RF input frequency range from 400

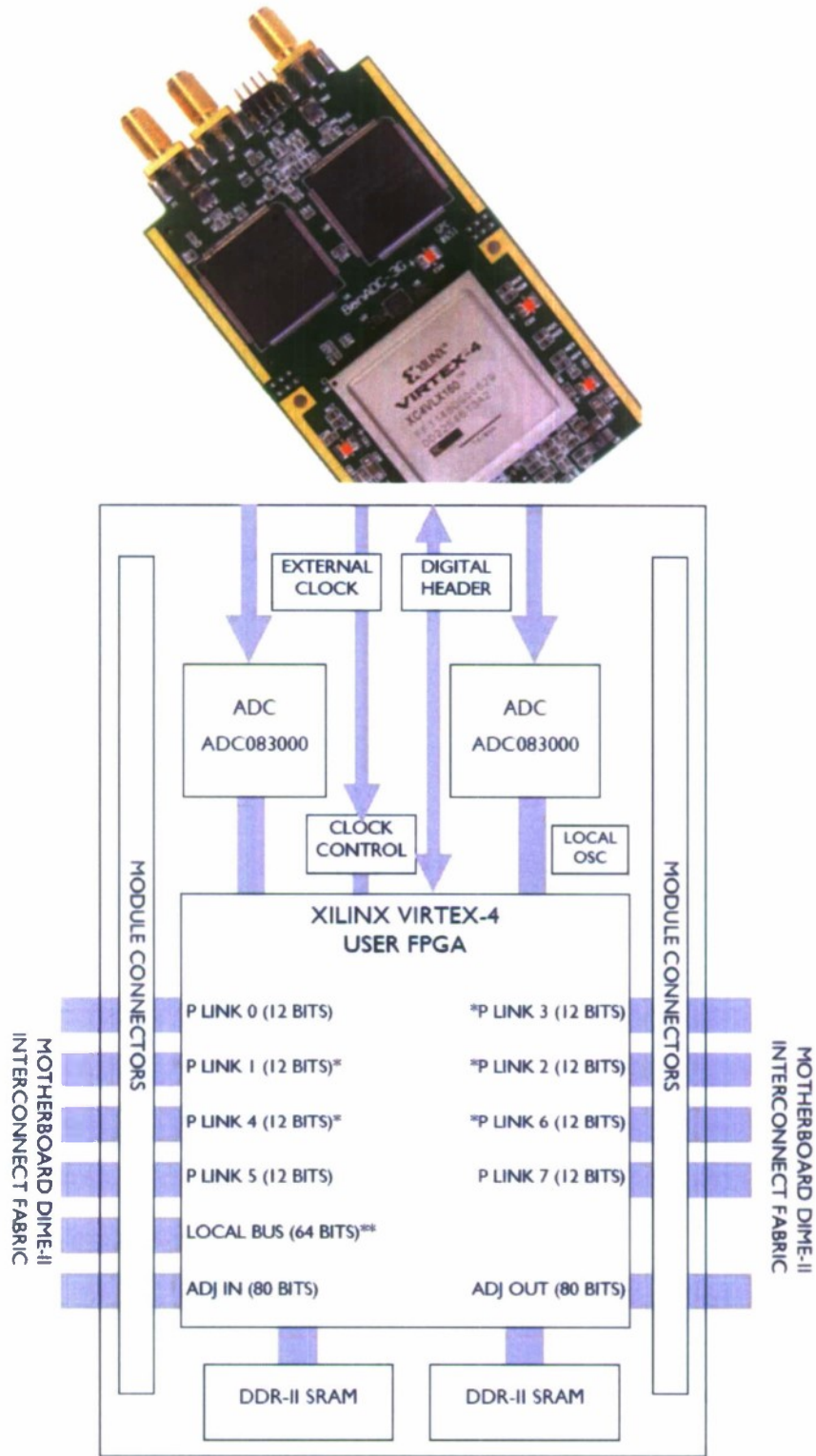


Figure 3.12: BenADC-3G board picture and functional diagram.

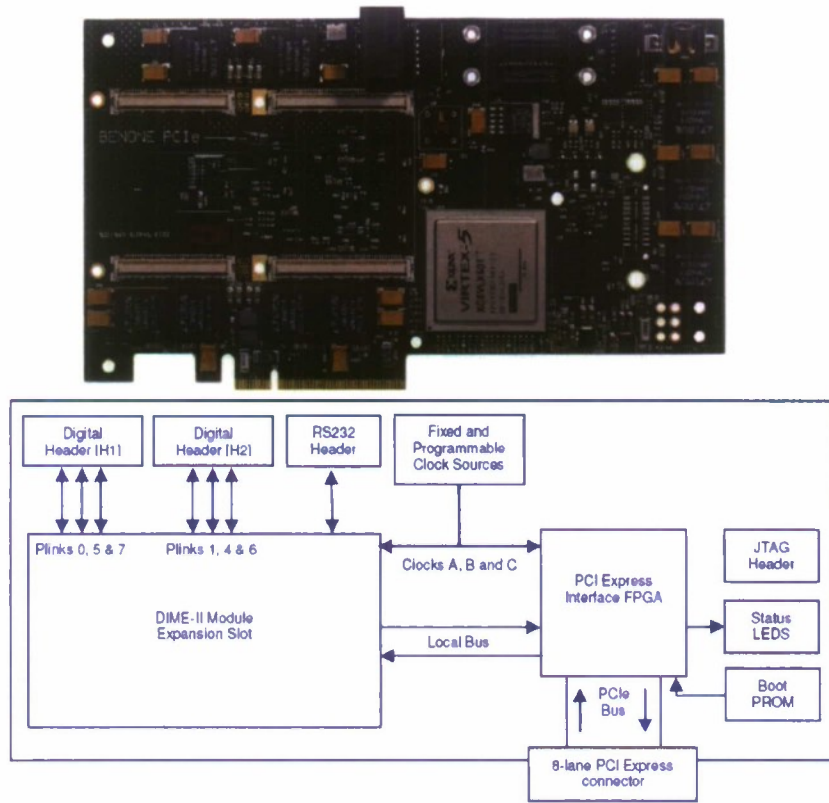


Figure 3.13: BenONE-PCIe board picture and functional diagram.

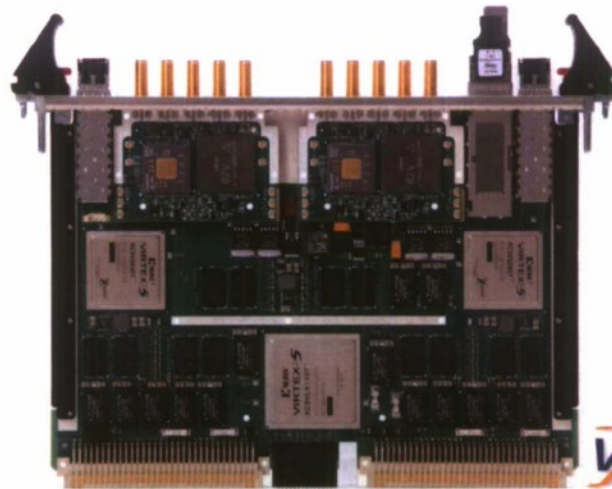


Figure 3.14: Neptune-V5 VXS board picture and functional diagram.

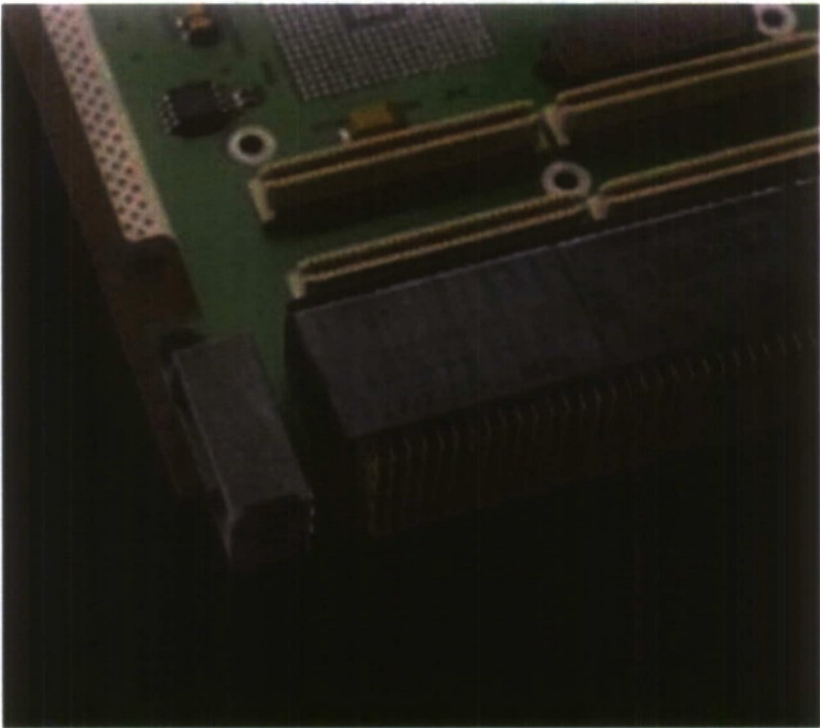


Figure 3.15: VSX connector picture.

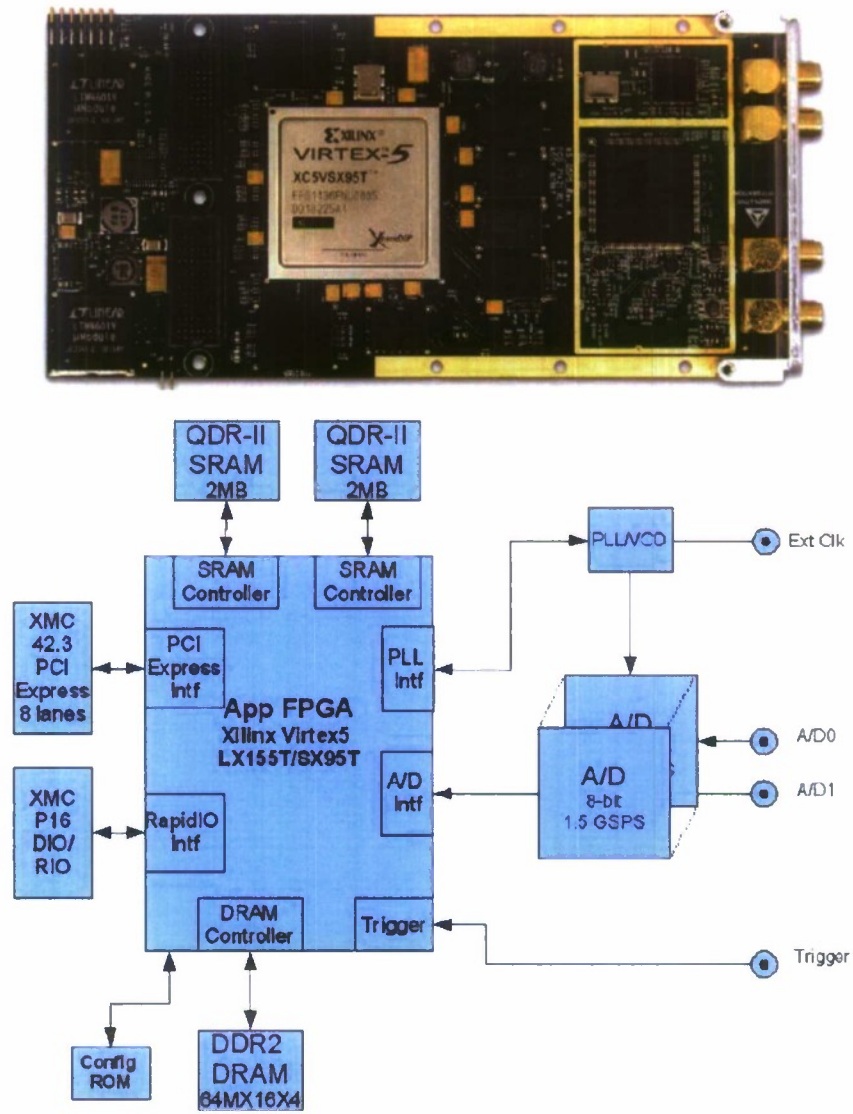


Figure 3.16: X5-GSPS board picture and functional diagram.

MHz to 6 GHz, With a NF = 13dB, IP1dB = 12dBm and IIP3 = 31dBm at 2.5GHz, the demodulator offers good dynamic range suitable for the demanding infrastructure direct-conversion requirements. The ADL5380 provides a typical voltage conversion gain of 4dB, helping to minimize the gain requirements of the receiver front end.

Figure 3.17 shows the diagram of the evaluation board schematics, where the differential RF inputs provide a well-behaved broad-band input impedance of 50Ω and be driven from a 1:1 balun for best performance. For the LO input interface, a 1:1 RF balun that converts the single-ended RF input to differential signal is used.

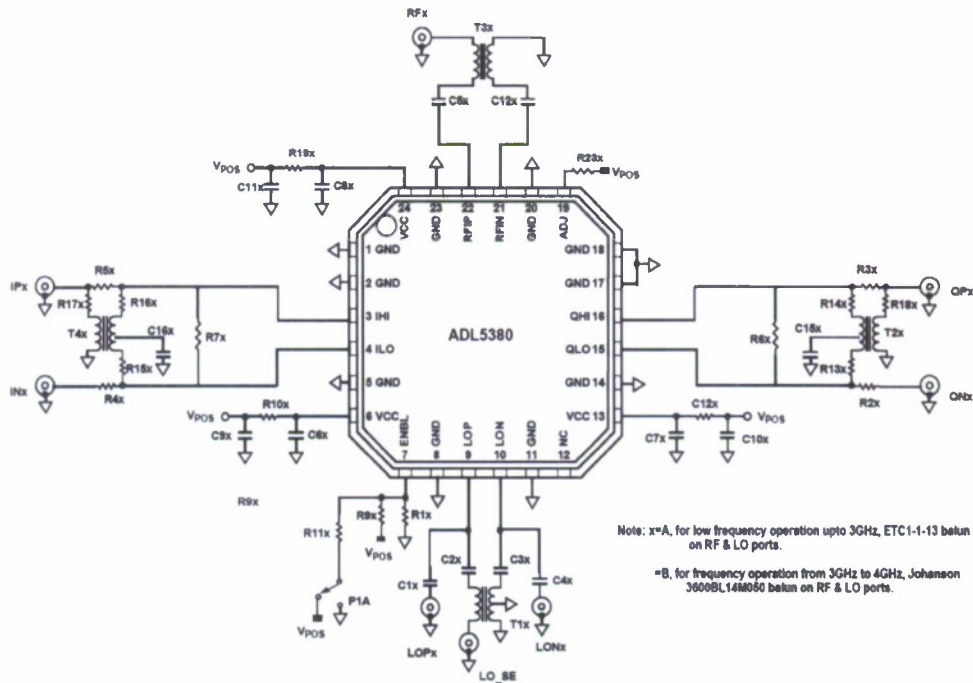


Figure 3.17: Diagram of ADL5380 Evaluation Board.

The baseband output of the evaluation board can be configured to Single-Ended output or full differential outputs. For single-ended, the baseband outputs are taken from QHI and IHI, R13x to R18x are populated for appropriate balun interface, and the balun TCM9-1 converts a differential high impedance IF output to a single-ended output, when loaded with 50Ω, this balun presents a 450Ω load to the device. For differential outputs, by populating R2x to R5x with 0Ω and not populating R13x to R18x. R2x to R5x provide a means to bypass the TCM9-1 transformer to allow for differential baseband outputs, the baseband outputs are taken from the SMAs of Q_HI, Q_LO, I_HI, and I_LO.

For the quadrature demodulation test, our setup is shown as Figure 3.18. At the transmitter side, the in-phase and quadrature baseband signals are generated by the DAC's waveform memory, then the signals are up-converted by the quadrature modulator ADL5375. The Local oscillator provide a 3.3 GHz carrier frequency for both the modulator and demodulator, where a power splitter is used. The modulator and demodulator are connected by a SMA cable to ensure appropriate RF signal level. A few of testing parameters are listed in table 3.1. Note that for differential output, we apply the R6 and R7 with 450 Ω to ensure the impedance balance, the measurement equipment has a impedance of 50Ω

Table 3.1: Quadrature demodulator ADL5380 testing setup and results

Baseband input in-phase	45 MHz Sinusoid	
Baseband input quadrature	45 MHz Sinusoid	
Phase of input signal	adjustable from 0 to 90	
LO center frequency	3.3GHz	
LO signal level	-6 dBm (Peak 320 mV)	
RF output level	-6 dBm (Peak 330 mV)	
Baseband output type	differential	Single-ended
Voltage and current	5V 170mA	5V 170mA
Baseband output in-phase	45 MHz Sinusoid	None
Baseband output quadrature	45 MHz Sinusoid	None
Peak-to-peak level of in-phase	70 mV	None
Peak-to-peak level of quadrature	190 mV	None
DC offset	2 V	2 V

In the testing process, we've found the following problem:

- (1) The baseband in-phase output is always at the level of 70 mV peak-to-peak value no matter how the baseband input phase changes, and the baseband quadrature output varies from 70 mVpp to 190 mVpp when the baseband input phase changes.
- (2) The working current is 170 mA instead of 240 mA as the datasheet indicates.
- (3) The Single-ended output has never been observed.

For the first problem may not be a real problem since the I/Q output imbalance may be reduced by adjusting the local oscillation phase at the demodulator side.

For the second problem, we believe the ADL5380 chip was damaged.

For the third problem, when the baseband outputs are set as differential mode, the output signals will go through the Baluns, we believe the Baluns have no problem after careful checking, so the outputs may be too weak to be detected. it's also probably because the chip's damaged.

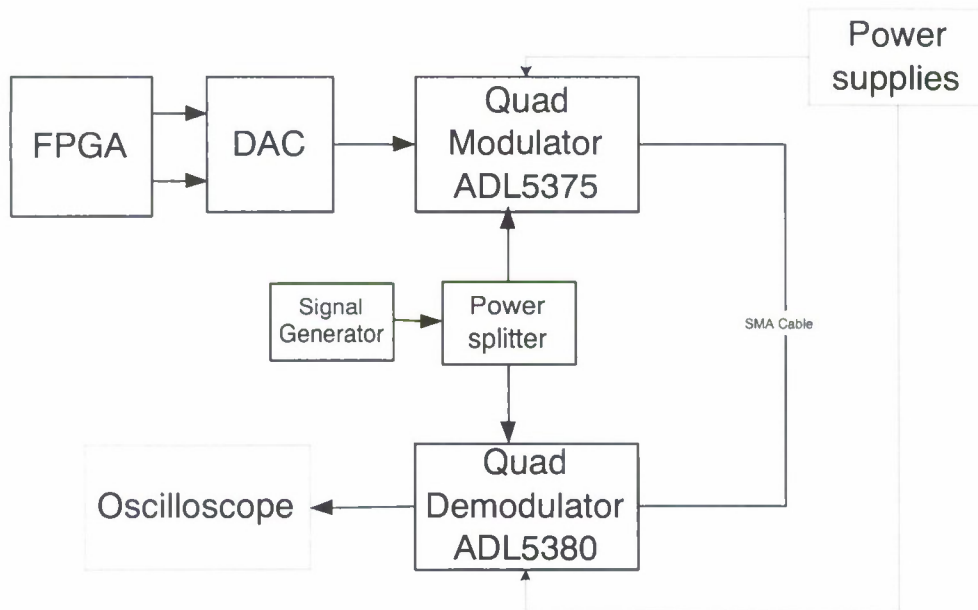


Figure 3.18: Testing setup for ADL5380 Evaluation Board.

Part II

Theoretical Work

Chapter 4

Wideband Waveform Optimization for Multiple Input Single Output (MISO) Cognitive Radio Using Time Reversal

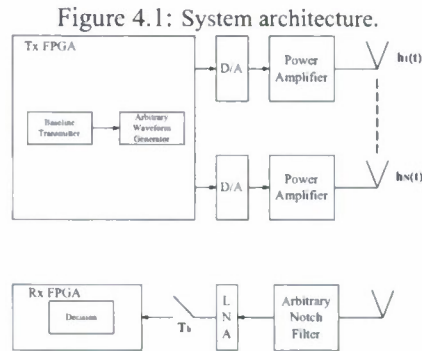
Waveform design or optimization is a key research issue in the current wireless communication system. Waveform should be designed according to the different requirements and objectives of system performance. For example, the waveform should be designed to carry more information to the receiver in terms of capacity. For navigation and geolocation, the ultra short waveform should be used to increase the resolution. If the energy detector is employed at the receiver, the waveform should be optimized such that the energy of the signal in the integration window at the receiver should be maximized [8] [9] [10] [11]. In the context of cognitive radio, waveform design or optimization give us more flexibilities to design radio, which can coexist with other cognitive radios and primary radios. From cognitive radio's point of view, spectral mask constraint at the transmitter and the influence of Arbitrary Notch Filter at the receiver should be seriously considered for waveform design or optimization, except the consideration of the traditional communication objectives. Spectral mask constraint is imposed on the transmitted waveform such that cognitive radio has no interference to primary radio. While Arbitrary Notch Filter at the receiver is used to cancel the interference from primary radio to cognitive radio.

4.1 Wideband Waveform Optimization

This section deals with wideband waveform optimization for multiple input single output (MISO) cognitive radio using time reversal. The system architecture is shown in Figure 4.1. We limit our discussion to a single user scenario. There are N antennas at the transmitter and one antenna at the receiver. OOK modulation is used for transmission. Thus the transmitted signal at the transmitter antenna n is,

$$s_n(t) = \sum_{j=-\infty}^{\infty} d_j p_n(t - jT_b) \quad (4.1)$$

where T_b is the bit duration, $p_n(t)$ is the transmitted bit waveform defined over $[0, T_p]$ at the transmitter antenna n and $d_j \in \{0, 1\}$ is j -th transmitted bit. Without loss of generality, the minimal propagation delay is assumed to be



zero. The energy of transmitted waveforms is E_p ,

$$\sum_{n=1}^N \int_0^{T_p} p_n^2(t) dt = E_p \quad (4.2)$$

The received noise-polluted signal at the output of low noise amplifier (LNA) is,

$$r(t) = \sum_{n=1}^N h_n(t) \otimes s_n(t) + n(t) \quad (4.3)$$

$$= \sum_{j=-\infty}^{\infty} d_j \sum_{n=1}^N x_n(t - jT_b) + n(t) \quad (4.4)$$

where $h_n(t)$, $t \in [0, T_h]$ is the multipath impulse response that takes into account the effect of channel impulse response, the RF front-ends in the transceivers such as Power Amplifier, LNA and Arbitrary Notch Filter as well as antennas between the transmitter antenna n and the receiver antenna. $h_n(t)$ is available at the transmitter. $\int_0^{T_h} h_n^2(t) dt = E_{nh}$. “ \otimes ” denotes convolution operation. $n(t)$ is AWGN. $x_n(t)$ is the received noiseless bit-“1” waveform defined as

$$x_n(t) = h_n(t) \otimes p_n(t) \quad (4.5)$$

We further assume that $T_b \geq T_h + T_p \stackrel{\text{def}}{=} T_x$, i.e. no existence of ISI.

If the waveforms at different transmitter antennas are assumed to be synchronized, the k -th decision statistic is,

$$r(kT_b + t_0) = \sum_{j=-\infty}^{\infty} d_j \sum_{n=1}^N x_n(kT_b + t_0 - jT_b) + n(t) \quad (4.6)$$

$$= d_k \sum_{n=1}^N x_n(t_0) + n(t) \quad (4.7)$$

In order to maximize the system performance, $\sum_{n=1}^N x_n(t_0)$ should be maximized. Thus the optimization problem can

be formulated as follows to get the optimal waveforms $p_n(t)$,

$$\begin{aligned} & \max \sum_{n=1}^N x_n(t_0) \\ & \text{s.t. } \sum_{n=1}^N \int_0^{T_p} p_n^2(t) df \leq E_p \\ & \quad 0 \leq t_0 \leq T_b \end{aligned} \quad (4.8)$$

An iterative algorithm is proposed here to give the optimal solution to the optimization problem, which is a computationally efficient algorithm. For the simplicity of the following presentation, t_0 is assumed to be zero. Meanwhile,

$$x(t) = \sum_{n=1}^N x_n(t) \quad (4.9)$$

From inverse Fourier transform,

$$x_{nf}(f) = h_{nf}(f) p_{nf}(f) \quad (4.10)$$

and

$$x_f(f) = \sum_{n=1}^N h_{nf}(f) p_{nf}(f) \quad (4.11)$$

where $x_{nf}(f)$, $h_{nf}(f)$ and $p_{nf}(f)$ are the frequency domain representations of $x_n(t)$, $h_n(t)$ and $p_n(t)$ respectively. $x_f(f)$ is frequency domain representation of $x(t)$. Thus,

$$x(0) = \sum_{n=1}^N x_n(0) \quad (4.12)$$

and,

$$x_n(0) = \int_{-\infty}^{\infty} x_{nf}(f) df \quad (4.13)$$

If there is no spectral mask constraint, then according to the Cauchy-Schwarz inequality,

$$x(0) = \sum_{n=1}^N \int_{-\infty}^{\infty} h_{nf}(f) p_{nf}(f) df \quad (4.14)$$

$$\leq \sum_{n=1}^N \sqrt{\int_{-\infty}^{\infty} |h_{nf}(f)|^2 df} \sqrt{\int_{-\infty}^{\infty} |p_{nf}(f)|^2 df} \quad (4.15)$$

$$\leq \sqrt{\sum_{n=1}^N \int_{-\infty}^{\infty} |h_{nf}(f)|^2 df} \sqrt{\sum_{n=1}^N \int_{-\infty}^{\infty} |p_{nf}(f)|^2 df} \quad (4.16)$$

$$= \sqrt{E_p \sum_{n=1}^N E_{nh}} \quad (4.17)$$

when $p_{nf}(f) = \alpha h_{nf}(f)$ for all f and n , two equalities are obtained.

$$\alpha = \sqrt{\frac{E_p}{\sum_{n=1}^N \int_{-\infty}^{\infty} |h_{nf}(f)|^2 df}} \quad (4.18)$$

In this case, $p_n(t) = \alpha h_n(-t)$, which means the optimal waveform $p_n(t)$ is the corresponding time reversed multipath impulse response $h_n(t)$.

If there is spectral mask constraint, then the following optimization problem will become more complicated,

$$\begin{aligned} & \max x(0) \\ & \text{s.t. } \sum_{n=1}^N \int_0^{T_p} p_n^2(t) df \leq E_p \\ & \quad |p_{nf}(f)|^2 \leq c_{nf}(f) \end{aligned} \quad (4.19)$$

where $c_{nf}(f)$ represents the arbitrary spectral mask constraint at the transmitter antenna n .

Because $p_{nf}(f)$ is the complex value, the phase and the modulus of $p_{nf}(f)$ should be determined.

Meanwhile,

$$x(0) = \int_{-\infty}^{\infty} x_f(f) df \quad (4.20)$$

and,

$$x_f(f) = \sum_{n=1}^N |h_{nf}(f)| |p_{nf}(f)| e^{j2\pi(\arg(h_{nf}(f)) + \arg(p_{nf}(f)))} \quad (4.21)$$

where the angular component of the complex value is $\arg(\bullet)$.

For the real value signal $x(t)$,

$$x_f(f) = x_f^*(-f) \quad (4.22)$$

where “*” denotes conjugate operation. Thus,

$$x_f(-f) = \sum_{n=1}^N |h_{nf}(f)| |p_{nf}(f)| e^{-j2\pi(\arg(h_{nf}(f)) + \arg(p_{nf}(f)))} \quad (4.23)$$

and $x_f(f) + x_f(-f)$ is equal to

$$\sum_{n=1}^N |h_{nf}(f)| |p_{nf}(f)| \cos(2\pi(\arg(h_{nf}(f)) + \arg(p_{nf}(f)))) \quad (4.24)$$

If $h_{nf}(f)$ and $|p_{nf}(f)|$ are given for all f and n , maximization $x(0)$ is equivalent to setting,

$$\arg(h_{nf}(f)) + \arg(p_{nf}(f)) = 0 \quad (4.25)$$

which means the angular component of $p_{nf}(f)$ is the negative angular component of $h_{nf}(f)$.

The optimization problem (4.19) can be simplified as,

$$\begin{aligned} & \max \sum_{n=1}^N \int_{-\infty}^{\infty} |h_{nf}(f)| |p_{nf}(f)| df \\ & \text{s.t. } \sum_{n=1}^N \int_{-\infty}^{\infty} |p_{nf}(f)|^2 df \leq E_p \\ & \quad |p_{nf}(f)|^2 \leq c_{nf}(f) \end{aligned} \quad (4.26)$$

Because,

$$|h_{nf}(f)| = |h_{nf}(-f)| \quad (4.27)$$

$$|p_{nf}(f)| = |p_{nf}(-f)| \quad (4.28)$$

$$|c_{nf}(f)| = |c_{nf}(-f)| \quad (4.29)$$

for all f and n . Thus uniformly discrete frequency points f_0, \dots, f_M are considered in the optimization problem (4.26). Meanwhile, f_0 corresponds to the DC component and f_1, \dots, f_M correspond to the positive frequency components.

Define column vectors $\mathbf{h}_f, \mathbf{h}_{1f}, \dots, \mathbf{h}_{Nf}$,

$$\mathbf{h}_f = [\mathbf{h}_{1f}^T \mathbf{h}_{2f}^T \cdots \mathbf{h}_{Nf}^T]^T \quad (4.30)$$

$$(\mathbf{h}_{nf})_i = \begin{cases} |h_{nf}(f_{i-1})|, & i = 1 \\ \sqrt{2} |h_{nf}(f_{i-1})|, & i = 2, \dots, M+1 \end{cases} \quad (4.31)$$

where “ T ” denotes transpose operation

Define column vectors $\mathbf{p}_f, \mathbf{p}_{1f}, \dots, \mathbf{p}_{Nf}$,

$$\mathbf{p}_f = [\mathbf{p}_{1f}^T \mathbf{p}_{2f}^T \cdots \mathbf{p}_{Nf}^T]^T \quad (4.32)$$

$$(\mathbf{p}_{nf})_i = \begin{cases} |p_{nf}(f_{i-1})|, & i = 1 \\ \sqrt{2} |p_{nf}(f_{i-1})|, & i = 2, \dots, M+1 \end{cases} \quad (4.33)$$

Define column vectors $\mathbf{c}_f, \mathbf{c}_{1f}, \dots, \mathbf{c}_{Nf}$,

$$\mathbf{c}_f = [\mathbf{c}_{1f}^T \mathbf{c}_{2f}^T \cdots \mathbf{c}_{Nf}^T]^T \quad (4.34)$$

$$(\mathbf{c}_{nf})_i = \begin{cases} \sqrt{|c_{nf}(f_{i-1})|}, & i = 1 \\ \sqrt{2 |c_{nf}(f_{i-1})|}, & i = 2, \dots, M+1 \end{cases} \quad (4.35)$$

Thus, the discrete version of the optimization problem (4.26) is shown below,

$$\begin{aligned} & \max \mathbf{h}_f^T \mathbf{p}_f \\ & \text{s.t. } \|\mathbf{p}_f\|_2^2 \leq E_p \\ & \quad 0 \leq \mathbf{p}_f \leq \mathbf{c}_f \end{aligned} \quad (4.36)$$

An iterative algorithm is shown as follows.

1. Initialization: $P = E_p$ and \mathbf{p}_f^* is set to be all-0 column vector.
2. Solve the following optimization problem to get the optimal \mathbf{q}_f^* using Cauchy–Schwarz inequality.

$$\begin{aligned} & \max \mathbf{h}_f^T \mathbf{q}_f \\ & \text{s.t. } \|\mathbf{q}_f\|_2^2 \leq P \end{aligned} \quad (4.37)$$

3. Find i , such that $(\mathbf{q}_f^*)_i$ is the maximal value in the set $\left\{ (\mathbf{q}_f^*)_j \mid (\mathbf{q}_f^*)_j > (\mathbf{c}_f)_j \right\}$. If $\{i\} = \emptyset$, then the algorithm is terminated and $\mathbf{p}_f^* := \mathbf{p}_f^* + \mathbf{q}_f^*$. Otherwise go to step 4.

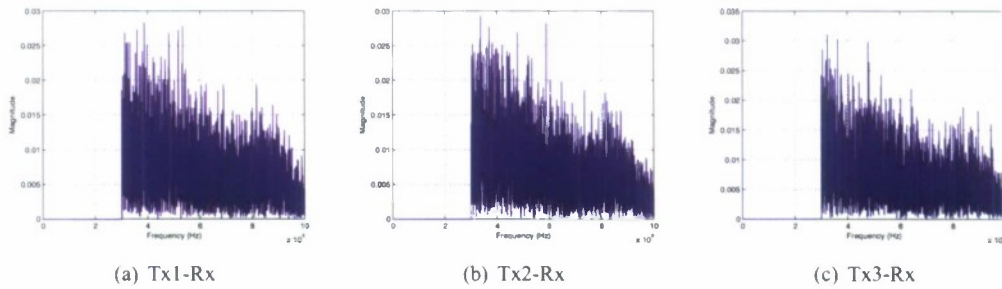


Figure 4.2: Channel transfer functions.

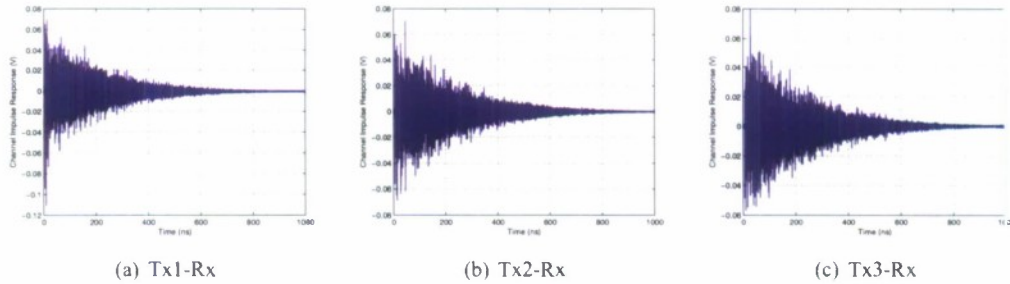


Figure 4.3: Channel impulse responses.

4. Set $(\mathbf{p}_f^*)_i = (\mathbf{c}_f)_i$.

5. $P := P - (\mathbf{c}_f)_i^2$ and set $(\mathbf{h}_f)_i$ to zero. Go to step 2.

When \mathbf{p}_f^* is obtained for the optimization problem (4.36), the optimal $p_{nf}(f)$ and the corresponding $I_n(t)$ can be smoothly achieved.

4.2 Numerical Results

The channel impulse responses in Rectangular Metal Cavity are used as an example to show the results of the wideband waveform optimization for MISO cognitive radio using time reversal. $N = 3$. The measured frequency band is from $3GHz$ to $10GHz$. Figure 4.2(a), Figure 4.2(b) and Figure 4.2(c) show channel transfer functions respectively. Figure 4.3(a), Figure 4.3(b) and Figure 4.3(c) show the corresponding channel impulse responses respectively. The energies of channel impulse responses are all normalized.

Because of the interference at the receiver, it is assumed that Arbitrary Notch Filter will notch the frequency band from $5GHz$ to $6GHz$ and the frequency band from $8GHz$ to $9GHz$. The transfer functions of the equivalent multipath impulse responses are shown in Figure 4.4(a), Figure 4.4(b) and Figure 4.4(c). Meanwhile, $E_{1h} = 0.7317$, $E_{2h} = 0.7451$ and $E_{3h} = 0.7278$.

Assume $E_p = 1$. If there is no spectral mask constraint or spectral mask constraint is not tight, the optimal waveform is the time reversed multipath impulse response. Figure 4.5(a), Figure 4.5(b) and Figure 4.5(c) show the spectral

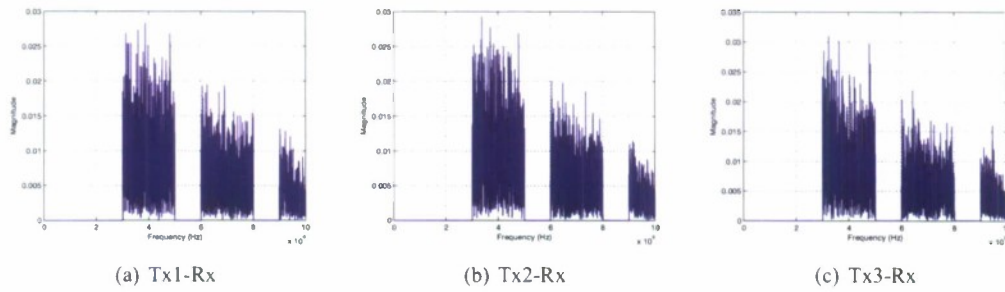


Figure 4.4: Transfer functions of multipath impulse response.

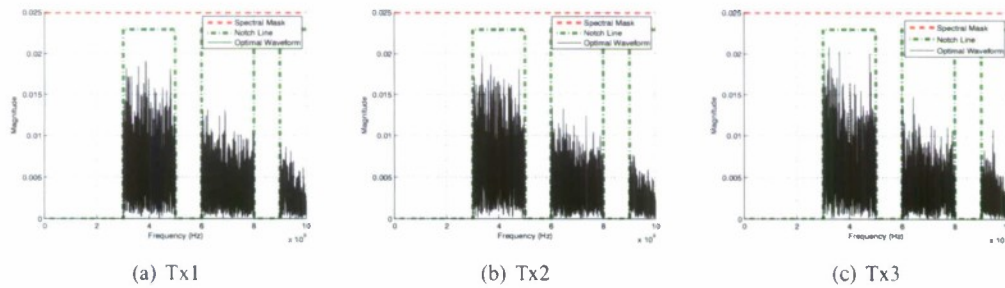


Figure 4.5: Spectral mask, notch line of Arbitrary Notch Filter and optimal waveform represented in the frequency domain.

masks and the optimal waveforms represented in the frequency domain for different antennas. Figure 4.6 shows $x(t)$ in Equation 4.9. The peak of $x(t)$ without noise in this case is 1.4848 which is equal to $\sqrt{E_p \sum_{n=1}^3 E_{nh}}$. If there is only one antenna at the transmitter, the peak of $x(t)$ without noise in this case is only 0.8554, 0.8632 or 0.8531.

If arbitrary spectral mask constrains are imposed on the different antennas, then the spectral masks and the optimal waveforms represented in the frequency domain for different antennas are shown in Figure 4.7(a), Figure 4.7(b) and Figure 4.7(c). Figure 4.8 shows $x(t)$ in Equation 4.9. The peak of $x(t)$ without noise in this case is 1.4777 which is very close to the optimal value without spectral mask constraint.

4.3 Discussion

This section deals with wideband waveform optimization for MISO cognitive radio using time reversal. Wideband waveform is designed according to the optimization objective with the considerations of spectral mask constraint at the transmitter and the influence of Arbitrary Notch Filter at the receiver. The numerical results make MISO time reversal a competent transmission scheme in the context of cognitive radio.

Figure 4.6: $x(t)$.

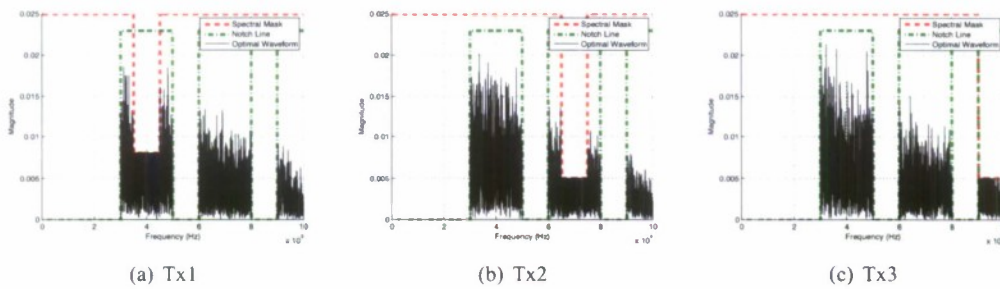
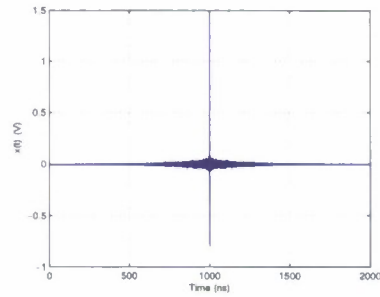
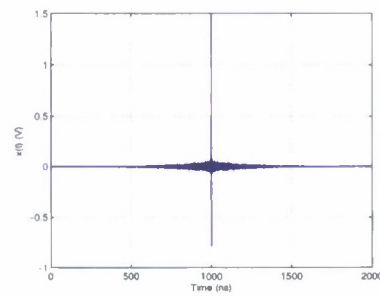


Figure 4.7: Spectral mask, notch line of Arbitrary Notch Filter and optimal waveform represented in the frequency domain.

Figure 4.8: $x(t)$.



Bibliography

- [1] P. Zhang, Z. Hu, R. Qiu, and B. Sadler, "A Compressed Sensing Based Ultra-Wideband Communication System," in *Proc. IEEE International Conference on Communications ICC '09*, pp. 1–5, 2009.
- [2] D. Donoho, "Compressed Sensing," *IEEE Transactions on Information Theory*, vol. 52, no. 4, pp. 1289–1306, 2006.
- [3] "Available online: <http://www.eweembedded.com/products/6/229/666.html>."
- [4] "Available online: <http://www.sundance.com/web/files/productpage.asp?strfilter=smt702>."
- [5] "Available online: <http://www.nallatech.com/index.php/modules/bcnade-3g.html>."
- [6] "Available online: www.tekmicro.com/pdfs/tekmicro.neptunev5.digitize.pdf."
- [7] "Available online: <http://www.innovative-dsp.com/products.php?product=x5-gsps>."
- [8] N. Guo, J. Q. Zhang, P. Zhang, Z. Hu, Y. Song, and R. C. Qiu, "UWB Real-Time Testbed with Waveform-Based Precoding," in *IEEE MILCOM'08*, 2008.
- [9] N. Guo, Z. Hu, A. S. Saini, and R. C. Qiu, "Waveform-level Precoding with Simple Energy Detector Receiver for Wideband Communication," in *IEEE SSST'09*, 2009.
- [10] Z. Hu, N. Guo, and R. C. Qiu, "Wideband Waveform Optimization for Energy Detector Receiver with Practical Considerations," in *IEEE ICUWB'09*, 2009.
- [11] Z. Hu, N. Guo, and R. C. Qiu, "Wideband Waveform Optimization with Energy Detector Receiver in Cognitive Radio," in *IEEE MILCOM'09*, 2009.